

# User driven quantum simulations with Rydberg atoms

Yannick Meurice

The University of Iowa  
with James Corona, Avi Kaufman, Zane Ozzello and M. Asaduzzaman  
QuLAT collaboration  
yannick-meurice@uiowa.edu

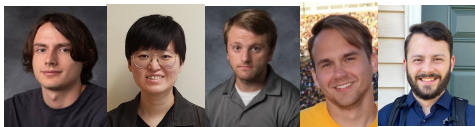
Supported by the Department of Energy under Award Number DOE DE-SC0019139 and DE-SC0010113

HHIQCD2024 YITP 11/14



# Students and postdocs

## U. Iowa Group



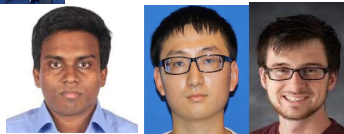
- **Undergrads:** Avi Kaufman, Aditya Venkatesh, Jaeho Kim
- **Grad. students:** James Corona, Zheyue Hang, Michael Hite, Zane Ozzello, Blake Senseman, ...
- **PostDocs:** M. Asaduzzaman, Jin Zhang (now Chongqing U.) and Kenny Heitritter (now qBraid)

## High-Energy Physics:

- B-meson decays with lattice gauge theory
- Composite models for the Higgs boson
- Applications of the Renormalization Group
- Tensor formulations of lattice field theory
- Machine learning in MC simulations

## Quantum computing:

- Real-time evolution of field theory models
- Quantum computing (IBMQ, trapped ions)
- Quantum simulations (Rydberg, QuEra)



## Former graduate students

- [Yuzhi Liu](#) (Ph. D. 2013): postdocs at U. Colorado Boulder and Indiana U.; Software engineer at Google
- [Haiyuan Zou](#) (Ph. D. 2014): postdocs at Pittsburgh U. and T. D. Lee Center; Assistant Prof. at East China Normal Un.
- [J. Unmuth-Yockey](#) (Ph. D. 2017): postdocs at Syracuse U. and Fermilab.
- [Z. Gelzer](#) (Ph. D. 2017): postdoc at U. Illinois UC.
- [D. Floor](#) (Ph. D. 2018), Software engineer in Brazil.
- [S. Foreman](#) (Ph. D. 2019): postdoc at Argonne Nat. Lab.
- [E. Gustafson](#) (Ph. D. 2021): postdoc at Fermilab
- [D. Simons](#) (Ph. D. 2023); [R. Maxton](#) (Ph. D. 2023)



# QuLAT Collaboration

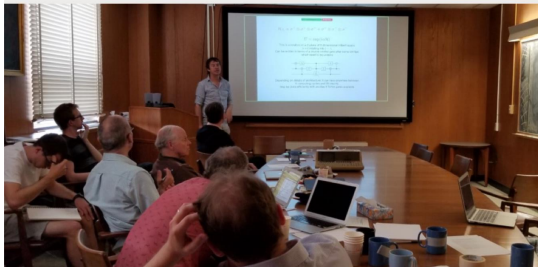
<https://qulat.sites.uiowa.edu/>

**IOWA**

Foundations of Quantum  
Computing for Gauge Theories and  
Quantum Gravity - The QuLAT  
Collaboration

About Abstract

Supported by the Department of Energy (QuantISED HEP)



## Goals of the collaboration

Quantum computers are expected to exceed the capacity of classical computers and to revolutionize several aspects of computation especially for the simulation of quantum systems. We develop new methods for using quantum computers to study aspects of the evolution of strongly interacting particles in collisions, the quantum behavior of gravitational systems and the emergence of space-time which are beyond the reach of classical computing. Our goal is to design the building blocks of universal quantum computers relevant for these problems and develop algorithms which scale reasonably with the size of the system.

## Principal Investigators

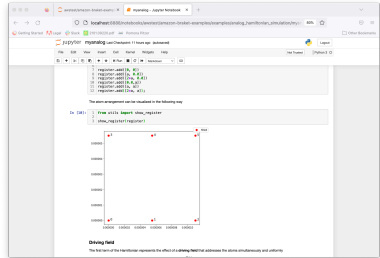
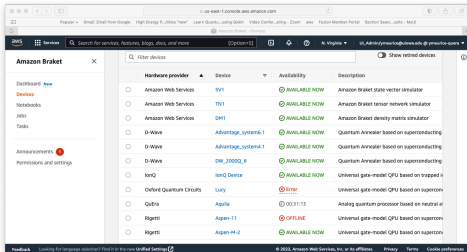
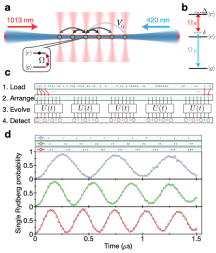
Alexei Bazavov, Michigan State University  
David Berenstein and Xi Dong, UCSB  
Richard Brower, Boston University  
Simon Catterall, Jay Hubisz, Alex Maloney  
Jason Pollack, Syracuse University  
Patrick Dreher, NCSU  
Yannick Meurice, Univ. of Iowa (Spokesperson)



# Contents

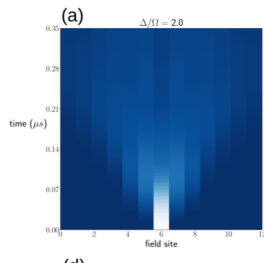
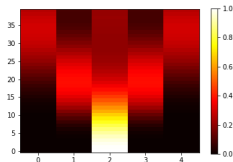
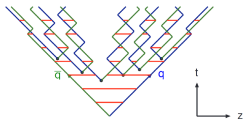
- Short review of the compact Abelian Higgs Model (Scalar QED) and its Rydberg atom simulator (PRD 104, 094513 (2021))
- Effective theory for the simulator (with J. Zhang and S.W. Tsai PRD 110, 034513 (2024))
- Phase diagram of the simulator
- First experimental observation of a floating phase (with QuEra, J. Zhang and S.W. Tsai, arXiv 2401.08087)
- Estimation of entanglement using mutual information of experimental bitstrings (arXiv 2404.09935)
- Improved entanglement estimators using “filtered” probabilities (arXiv 2411.07092)
- Asymptotic behavior of low probabilities (divergent in a non-normalizable way in the infinite volume limit?)
- Classical competition for real-time evolution: HOTRG (arXiv 2411.05301)





# Hybrid hadronization in event generators?

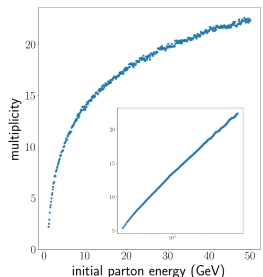
Lund String Fragmentation Model



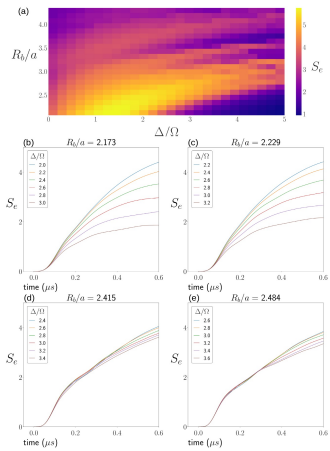
Evolution of a particle-antiparticle pair with the Lund model/Pythia (left), the Abelian Higgs model in 1+1 dimensions (middle), and a Rydberg atom simulator for this model (right).



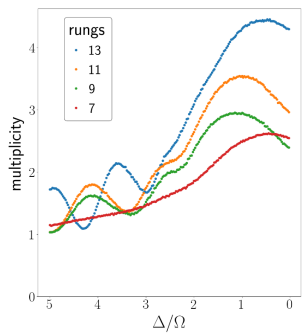
# Hadron Multiplicity (graph by K. Heitritter, 2212.02476)



Pythia/Lund



Entanglement Entropy (simulator)



First attempt on a small lattice with detuning playing the role of energy (see arxiv 2212.02476)



# Compact Abelian Higgs Model (CAHM)

The lattice compact Abelian Higgs model is a non-perturbative regularized formulation of scalar quantum electrodynamics (scalar electrons-positrons + photons with compact fields).

$$Z_{CAHM} = \prod_x \int_{-\pi}^{\pi} \frac{d\varphi_x}{2\pi} \prod_{x,\mu} \int_{-\pi}^{\pi} \frac{dA_{x,\mu}}{2\pi} e^{-S_{gauge} - S_{matter}},$$

$$S_{gauge} = \beta_{plaque} \sum_{x,\mu < \nu} (1 - \cos(A_{x,\mu} + A_{x+\hat{\mu},\nu} - A_{x+\hat{\nu},\mu} - A_{x,\nu})),$$

$$S_{matter} = \beta_{link} \sum_{x,\mu} (1 - \cos(\varphi_{x+\hat{\mu}} - \varphi_x + A_{x,\mu})).$$

- local invariance:  $\varphi'_x = \varphi_x + \alpha_x$  and  $A'_{x,\mu} = A_{x,\mu} - (\alpha_{x+\hat{\mu}} - \alpha_x)$ .
- $\varphi$  is the Nambu-Goldstone mode of the original model. The Brout-Englert-Higgs mode is decoupled (heavy).





# AHM: Hamiltonian and Hilbert space in 1+1 dim.

The continuous-time limit yields the Hamiltonian

$$H = \frac{U}{2} \sum_{i=1}^{N_s} (L_i^z)^2 + \frac{Y}{2} \sum_i (L_{i+1}^z - L_i^z)^2 - X \sum_{i=1}^{N_s} U_i^x$$

with  $U^x \equiv \frac{1}{2}(U^+ + U^-)$  and  $L^z|m\rangle = m|m\rangle$  and  $U^\pm|m\rangle = |m \pm 1\rangle$ .

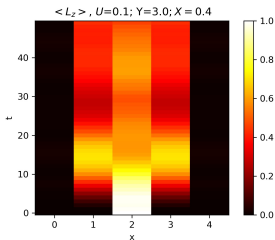
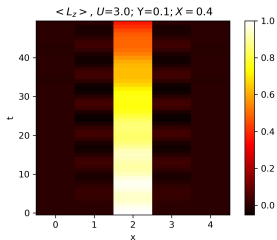
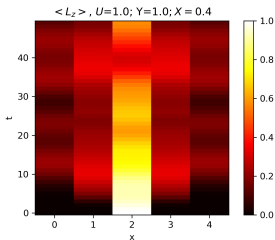
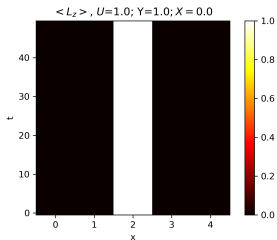
- $m$  is a discrete electric field quantum number ( $-\infty < m < +\infty$ )
- In practice, we need to apply truncations:  $U^\pm|\pm m_{max}\rangle = 0$ .
- We focus on the spin-1 truncation ( $m = \pm 1, 0$  and  $U^x = L^x/\sqrt{2}$ .)
- $U$ -term: electric field energy.
- $Y$ -term: matter charges (determined by Gauss's law)
- $X$ -term: currents inducing temporal changes in the electric field.



# Target simulations (E-field, spin-1, 5 sites)

$$H = \frac{U}{2} \sum_{i=1}^{N_s} (L_i^z)^2 + \frac{Y}{2} \sum_i (L_{i+1}^z - L_i^z)^2 - X \sum_{i=1}^{N_s} U_i^x$$

Initial state: particle-antiparticle (connected by an electric field +1)



# Qutrit Trotter implementation (M. Asaduzzaman)

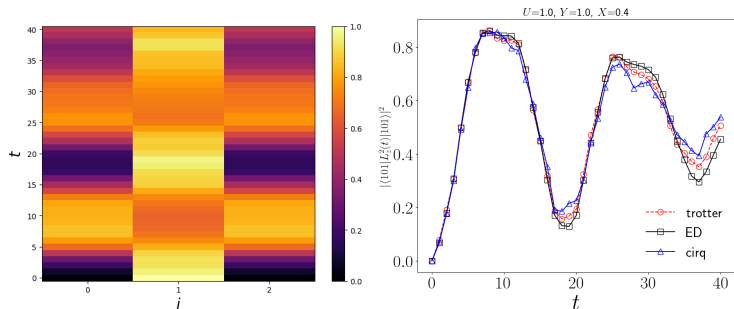


**Figure:** Left: Trotter evolution of the electric field in 3-spin scalar QED. Right: Comparison with ED and Cirq for the left site (M. Asaduzzaman). Experimental work in progress with M. Blok group (Rochester) plus N. Cross and R. Naik (Advanced Quantum Testbed, LBNL).



# Configurable Arrays of Rydberg Atoms (CARA)

- One can adapt (Y.M., PRD 104) the optical lattice construction (J. Zhang et al. PRL 121, A. Bazavov et al. PRD 92) using  $^{87}\text{Rb}$  atoms separated by controllable (but not too small) distances, coupled to the **excited Rydberg state**  $|r\rangle$  with a detuning  $\Delta$  to quantum simulate the Abelian Higgs model.
- **The ground state is denoted  $|g\rangle$  and the two possible states  $|g\rangle$  and  $|r\rangle$  can be seen as a qubit.  $n|g\rangle = 0$ ,  $n|r\rangle = |r\rangle$ .**
- The Hamiltonian reads

$$H = \frac{\Omega}{2} \sum_i (|g_i\rangle\langle r_i| + |r_i\rangle\langle g_i|) - \Delta \sum_i n_i + \sum_{i < j} V_{ij} n_i n_j,$$

with

$$V_{ij} = \Omega R_b^6 / r_{ij}^6,$$

for a distance  $r_{ij}$  between the atoms labelled as  $i$  and  $j$ . Note: when  $r = R_b$ ,  $V = \Omega$ .

- **This repulsive interaction prevents two atoms close enough to each other to be both in the  $|r\rangle$  state (blockade mechanism)**



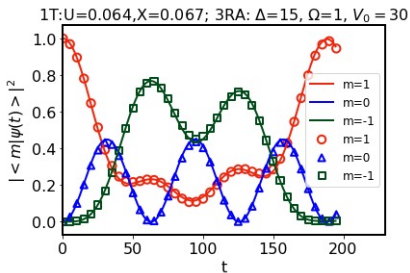
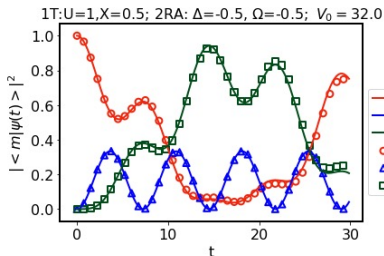
# One site spin-1 with 2 and 3 atoms (Y.M. PRD 104)

●  $|r\rangle$    ○  $|g\rangle$    ○  $|g\rangle$

●  $|r\rangle$    ○  $|g\rangle$    ○  $|g\rangle$

○  $|g\rangle$    ○  $|g\rangle$    ●  $|r\rangle$   
 $|rg\rangle$     $|gg\rangle$     $|gr\rangle$   
 $m=1$     $m=0$     $m=-1$

○  $|g\rangle$    ●  $|r\rangle$    ○  $|g\rangle$   
 $|rgg\rangle$     $|grg\rangle$     $|ggr\rangle$   
 $m=1$     $m=0$     $m=-1$



Solid line: target, Symbols: simulator



# QuEra (as seen by users)

```
[2]: from braket.aws import AwsDevice
from pprint import pprint as pp

device = AwsDevice("arn:aws:braket:us-east-1::device/qpu/quera/Aquila")
```

```
register = AtonArrangement()
ax = 4e-6 # meters
ay = 8e-6
ns=5
nl=2
for xx in range(ns):
    for yy in range(nl):
        register.add([xymax,yyay])
show_register(register)

$show_register(register, show_aton_index=False, blockade_radius=1.5 * separation)
```

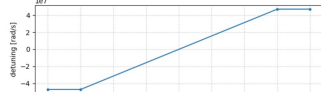


```
[22]: print("Quantum Task Summary")
print(tracker.quantum_tasks_statistics())
print('Note: Charges shown are estimates based on your Amazon Braket simulator and quantum processing unit (QPU) ta:
print(f"Estimated cost to run this example: {tracker.qpu_tasks_cost() + tracker.simulator_tasks_cost():.2f} USD")
```

```
Quantum Task Summary
{'arn:aws:braket:us-east-1::device/qpu/quera/Aquila': {'shots': 100, 'tasks': {'COMPLETED': 1}}}
Note: Charges shown are estimates based on your Amazon Braket simulator and quantum processing unit (QPU) task usag:
ts, and you may experience additional charges based on your use of other services such as Amazon Elastic Compute Cl:
Estimated cost to run this example: 1.30 USD
```

[6]: `fit += drive`

```
from qiskit import show_global_drive
show_global_drive(drive)
```



```
[23]: def get_counters_from_result(result):
    post_sequences = [list(measurement.post_sequence) for measurement in result.measurements]
    post_sequences = ["".join(['r' if site==0 else 'g' for site in post_sequence]) for post_sequence in post_sequences]
    counters = {}
    for post_sequence in post_sequences:
        if post_sequence in counters:
            counters[post_sequence] += 1
        else:
            counters[post_sequence] = 1
    return counters
get_counters_from_result(result)
```

```
[23]: {'grrggrrr': 1,
      'rggggrrr': 7,
      'grrggrrg': 7,
      'rrgggrrg': 6,
      'rrgggrrg': 4,
      'grrggrrr': 8,
      'rrggrrrg': 1,
      'rgrrgggr': 2,
      'rrggrrrg': 2,
      'rrggrrrg': 1,
      'rgrrrrgr': 1,
      'rgrrrrgr': 2,
      'rgrrrrgr': 1,
```



# Phase diagrams with lobes

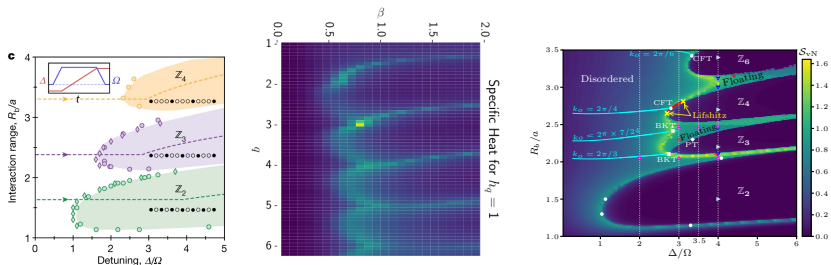


**Figure:** Left: The phase diagram of a single chain quantum simulator with continuously tunable parameters, composed of Rydberg atoms in a study of the Kimble-Zurek mechanism (Keesling et al.). Middle: A heatmap of the specific heat from the Extended-O(2) model with a symmetry-breaking  $h_q \cos(q\phi)$  (Hostetler, Bazavov et al., PRD 109, 054514 (2024)). Right: Phase diagram for the Rydberg ladder (Zhang et al., arXiv 2401.08087 ).



# Work with experimentalists

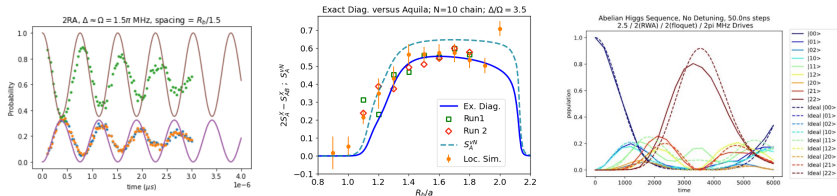


**Figure:** Left: Beta test of QuEra for two atoms starting in the ground state. Middle: Entanglement proxy  $2S_A^X - S_{AB}^X$  vs.  $R_b/a_x$  with three methods described in arXiv 2404.09935, empty symbols are Aquila results with 1000 shots (tomorrow's seminar); Right: Example of Floquet engineering for the two qutrit systems developed by M. Blok with undergraduate student Max Niederbach and Ray Parker. The dash lines correspond to a simulation with QuTIP including noise that they expect to implement on their facilities, while the continuous lines are obtained with exact diagonalization.





QuLAT had 2 awards: simulations on hyperbolic spaces (Goksu Con Toga), multipartite entanglement in 2D arrays (YM).

HOME ABOUT SCIENCE SYSTEMS FOR USERS NEWS **R & D** EVENTS LIVE STATUS

R & D

- Superfacility
- Data Analytics
- Quantum@NERSC
- Quantum Information Science @ Perlmutter
- Quantum Computing Access @ NERSC**
- NESAP
- Advanced Technologies Research at NERSC
- NERSC proxy suite
- HPC Requirements Reviews

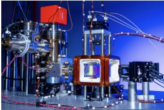
Home » R & D » Quantum@NERSC » Quantum Computing Access @ NERSC

## QUANTUM COMPUTING ACCESS @ NERSC

The Quantum Computing Access @ NERSC (QCAN) program is a first-of-its-kind program to support research on one of the first publicly accessible quantum computers based on neutral atom technology.

Through a partnership between QuEra Computing, competitive proposals are awarded up to 25 hours of quantum computer time, or 270,000 shots, on the company's **Aquila neutral atom system**.

NERSC and QuEra staff engage deeply with researchers during the project, including biweekly meetings to ensure project goals are met.



The magneto optical trap at the heart of QuEra's Aquila, a neutral atom system made available to researchers through the QCAN program. (Credit: QuEra Computing)

### Why Neutral Atom Systems?

Neutral atom quantum computers offer distinct advantages in scale and coherence time. Aquila, a 256-qubit analog quantum simulator, can simulate time evolution under the many-body Rydberg Hamiltonian. [A white paper on Aquila](#) describes the system's technical details, including prototypical use cases.



# Teaching quantum mechanics with public quantum devices?

It is possible to implement “gedanken experiments” in Feynman, Sakurai and Townsend textbooks using universal quantum computers

## 6 A MODERN APPROACH TO QUANTUM MECHANICS

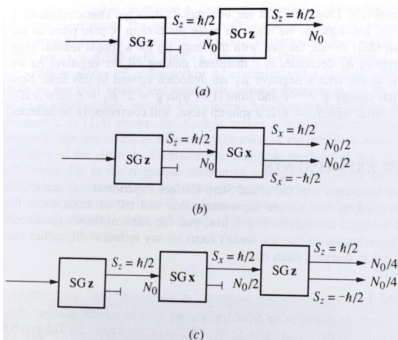


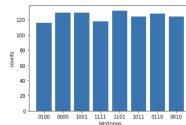
FIGURE 1.3 A block diagram of (a) Experiment 1, (b) Experiment 2, and (c) Experiment 3.  $N_0$  is the number of particles in the beam exiting the first SG device with  $S_z = \hbar/2$ .

```
In [17]: 1 #Experiment 3
2 mc1 = Circuit().h(0).cnot(0,1).ry(0,-np.pi/2).cnot(0,2).ry(0,np.pi/2).cnot(0,3)
3 print(mc1)
4 # run circuit
5 nshots=1000
6 result = device.run(mc1, shots=nshots).result()
7 # get measurement shots
8 counts = result.measurement_counts
9 # print counts
10 print(counts)
11 # plot using Counter
12 plt.bar(counts.keys(), counts.values())
13 plt.xlabel('bitstrings')
14 plt.ylabel('counts')
```

```
T : |0>|1> 2 |3> 4 |5>
q0 : H-C-Ry(-1.57)-C-Ry(1.57)-C-
q1 : X-----X-----
q2 : -----X-----
q3 : -----X-----
```

```
T : |0>|1> 2 |3> 4 |5>
Counter({'1101': 132, '0000': 129, '1001': 129, '0110': 126, '1011': 124, '0010': 124, '1111': 118, '0100': 116})
```

Out[17]: Text(0, 0.5, 'counts')



# Effective Hamiltonian (with J. Zhang and S. W. Tsai)

represent the four projected states in the  $z$  direction for spin  $3/2$ ; then, the on-rung interaction can be expressed by  $\sum_{u=0}^3 A_u (\hat{L}_i^z)^u$ , where the coefficients  $A_u$  can be found by matching the energy spectrum. However, in real quantum systems, the most common onsite terms are the linear term, which is coupled to the external field, and the quadratic term, which is the single-ion anisotropy. In addition, the Rydberg interaction is strong when the rung size is smaller than the Rydberg blockade radius, such that the  $|r_{i,1} r_{i,2}\rangle$  state is not likely to appear. Here we only consider a spin-1 realization by mapping the first three states to the spin-1 projected states  $|0\rangle$ ,  $|+1\rangle$ , and  $|-1\rangle$ , respectively. The onsite interaction term in spin language is thus  $-\Delta(\hat{L}_i^z)^2$ . The relation of the  $z$ -component spin operator to the Rydberg number operator is defined as [15]

$$\hat{L}_i^z = \hat{n}_{i,+1} - \hat{n}_{i,-1}. \quad (6)$$

If we take the square of this equation, use the property  $\hat{n}^2 = \hat{n}$ , and drop the term  $\hat{n}_{i,+1}\hat{n}_{i,-1}$ , which is zero in the low-energy sector, we obtain effectively

$$(\hat{L}_i^z)^2 = \hat{n}_{i,+1} + \hat{n}_{i,-1}. \quad (7)$$

Solving for  $\hat{n}_{i,m}$ , we get

$$\hat{n}_{i,+1(-1)} = [(\hat{L}_i^z)^2 \pm \hat{L}_i^z]/2. \quad (8)$$

between atoms in different legs  $V_2 = V_0\rho^6/(1+\rho^2)^3$ . The interactions between the  $(i, i+1)$  rungs are

$$\hat{H}_{2L,R,NN} = \frac{V_1 - V_2}{2} \hat{L}_i^z \hat{L}_{i+1}^z + \frac{V_1 + V_2}{2} (\hat{L}_i^z)^2 (\hat{L}_{i+1}^z)^2. \quad (9)$$

For generic values of  $\rho$ , it is necessary to include the long-range interactions. The interactions between the spin at site  $i$  and that at site  $i+k$  take the same form as Eq. (9) by replacing  $V_1, V_2$  by  $V_1^{(k)} = V_0\rho^6/k^6$ ,  $V_2^{(k)} = V_0\rho^6/(k^2 + \rho^2)^3$ .

Finally, we note that the Rydberg Rabi term can flip the spin projections between  $|0\rangle$  and  $|\pm 1\rangle$ , but there is no direct flipping channel between  $|+1\rangle$  and  $|-1\rangle$ , where the Rabi term is equivalent to the spin-1 ladder operator. In summary, if the rung size of the two-leg ladder is smaller than the Rydberg blockade radius, or  $V_0 \gg \Delta, \Omega$ , the two-leg Rydberg ladder is an effective spin-1 chain:

$$\begin{aligned} \hat{H}_{2L,R}^{\text{eff}} = & -\Delta \sum_{i=1}^{N_s} (\hat{L}_i^z)^2 + \sum_k \left( \frac{V_1^{(k)} - V_2^{(k)}}{2} \sum_{i=1}^{N_s-k} \hat{L}_i^z \hat{L}_{i+k}^z \right. \\ & \left. + \frac{V_1^{(k)} + V_2^{(k)}}{2} \sum_{i=1}^{N_s-k} (\hat{L}_i^z)^2 (\hat{L}_{i+k}^z)^2 \right) \\ & + \frac{\Omega}{2} \sum_{i=1}^{N_s} (\hat{U}_i^+ + \hat{U}_i^-). \end{aligned} \quad (10)$$

We now consider the case where the long-range interactions have a negligible effect and keep only the



# Comparison between ladder $H_{eff.}$ and $H_{CAHM}$

Phys.Rev.D 110 (2024) 3, 034513 arXiv 2312.04436

$$H_{CAHM} = \frac{U}{2} \sum_{i=1}^{N_s} (L_i^Z)^2 - Y \sum_{i=1}^{N_s-1} L_{i+1}^Z L_i^Z - X \sum_{i=1}^{N_s} U_i^X$$

$$H_{eff.} = -\Delta \sum_{i=1}^{N_s} (L_i^Z)^2 + \frac{V_1 - V_2}{2} \sum_{i=1}^{N_s-1} L_i^Z L_{i+1}^Z + \Omega \sum_{i=1}^{N_s} U_i^X + H_{quartic}$$

$$H_{quartic} = \frac{V_1 + V_2}{2} \sum_{i=1}^{N_s-1} (L_i^Z)^2 (L_{i+1}^Z)^2.$$

## Matching

- $\Delta = -U/2$  (sign matters!)
- The coefficient for  $L_i^Z L_{i+1}^Z$  is positive ( $V_1 > V_2$ ) for the simulator (repulsive/antiferromagnetic) but the CAHM has ferromagnetic interactions. This can be remedied by redefining the observable  $L_{2i+1}^Z \rightarrow -L_{2i+1}^Z$  (staggered)
- After redefinition  $V_1 = -V_2 = Y > 0$  but  $V_2 > 0$
- $\Omega = -X$  (sign does not matter)

Everything agrees with two-rung results (YM, PRD104)



# Effect of new quartic term (arXiv:2312.04436)

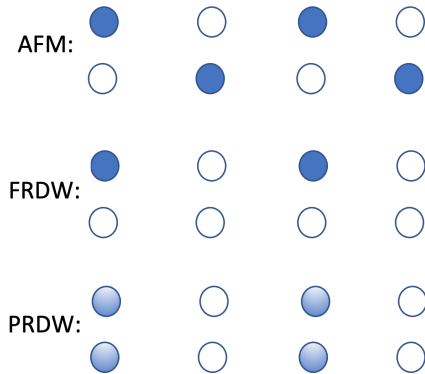
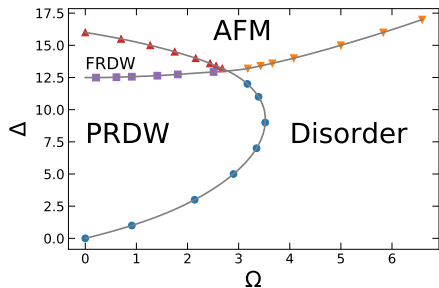


**Figure:** Ground-state phase diagram for the effective Hamiltonian of the two-leg Rydberg ladder. Here  $L = 512$ ,  $V_0 = 1000$ ,  $\rho = dy/dx = 0.5$ . The PRDW phase is disordered in even or odd sites, and the FRDW phase is FM in even or odd sites.



# Probing quantum floating phases in Rydberg atom arrays, arXiv:2401.08087, graphs by J. Zhang (th.) and S. Cantu (exp.)

## Probing quantum floating phases in Rydberg atom arrays

Jin Zhang<sup>1,2,\*</sup>, Sergio H. Cantu<sup>3,†</sup>, Fangli Liu<sup>3,‡</sup>, Alexei Bylinskii<sup>3</sup>, Boris Braverman<sup>3</sup>, Florian Huber<sup>3</sup>, Jesse Amato-Grill<sup>3</sup>, Alexander Lukin<sup>3</sup>, Nathan Gemelke<sup>3</sup>, Alexander Keesling<sup>3</sup>, Sheng-Tao Wang<sup>3</sup>, Y. Meurice<sup>1</sup>, and S.-W. Tsai<sup>4</sup>

<sup>1</sup>*Department of Physics and Astronomy, University of Iowa, Iowa City, IA 52242, USA*

<sup>2</sup>*Department of Physics and Chongqing Key Laboratory for Strongly Coupled Physics, Chongqing University, Chongqing 401331, China*

<sup>3</sup>*QuEra Computing Inc., 1284 Soldiers Field Road, Boston, MA, 02135, USA and*

<sup>4</sup>*Department of Physics and Astronomy, University of California, Riverside, CA 92521, USA*

(Dated: February 13, 2024)

The floating phase, a critical incommensurate phase, has been theoretically predicted as a potential intermediate phase between crystalline ordered and disordered phases. In this study, we investigate the different quantum phases that arise in ladder arrays comprising up to 92 neutral-atom qubits and experimentally observe the emergence of the quantum floating phase. We analyze the site-resolved Rydberg state densities and the distribution of state occurrences. The site-resolved measurement reveals the formation of domain walls within the commensurate ordered phase, which subsequently proliferate and give rise to the floating phase with incommensurate quasi-long-range order. By analyzing the Fourier spectra of the Rydberg density-density correlations, we observe clear signatures of the incommensurate wave order of the floating phase. Furthermore, as the experimental system sizes increase, we show that the wave vectors approach a continuum of values incommensurate with the lattice. Our work motivates future studies to further explore the nature of commensurate-incommensurate phase transitions and their non-equilibrium physics.



# Set up and phase diagram

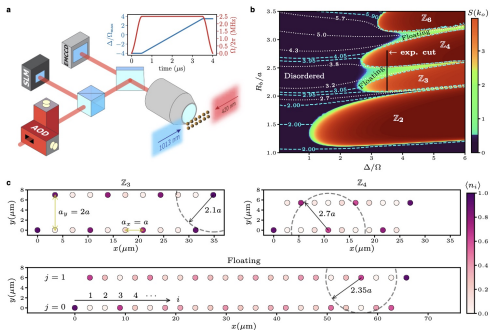


FIG. 1. **Quantum phases of Rydberg atoms arranged in a two-leg ladder.** a, Atoms are loaded into a two-leg ladder of optical tweezer traps generated using a SLM and rearranged into defect-free patterns by a second set of moving tweezers using a pair of crossed AODs. Coherent transitions are driven between the ground state  $|g\rangle = |\text{SS}\rangle_{1/2}$  and the Rydberg state  $|r\rangle = |\text{RS}\rangle_{1/2}$  in each atom with a two-photon transition induced by lasers at 420 nm and 1013 nm. The inset shows a linear detuning sweep  $\Delta(t)$  at a constant Rabi frequency  $\Omega_{\text{max}} = 2\pi \times 2.5$  MHz for preparing the ground states of the phase diagram via adiabatic evolution. Projection of the many-body quantum state into bitstrings of  $|g\rangle$  and  $|r\rangle$  for each atom can be detected on an EMCCD camera with the Rydberg state  $|r\rangle$  detected as loss of atom. b, The ground-state phase diagram for the Rydberg Hamiltonian [Eq. (1)] in a two-leg ladder is shown with lattice spacings  $a_x = a$  and  $a_y = 2a$ . Structure factors  $S(k)$  are numerically computed for  $1 \leq R_b/a \leq 3.5$  using DMRG (Supplementary Information). The color map depicts the peak height  $S(k_p)$  at  $k_p = 2\pi/p$  with  $p$  being the wavelength in units of the lattice constant  $a$ , while contour lines show the constant- $p$  lines. The  $Z_p$  orders have constant values of integer  $p$ , while the floating phase exhibits a continuously varying  $p$ . The black line cut corresponds to experimental parameters chosen in subsequent figures. c, Experimentally measured Rydberg densities illustrate the  $Z_p$  orders and the floating phase. The radius of the dashed circle illustrates the Rydberg blockade radius  $R_b$ . The  $Z_3$  and  $Z_4$  orders exhibit Rydberg density oscillations with periods of  $p = 3$  and  $p = 4$  lattice spacings, respectively. The incommensurate floating phase displays no discernible periodicity in density oscillations.

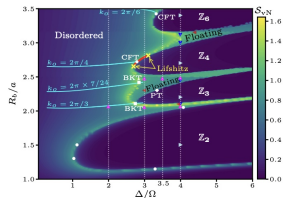
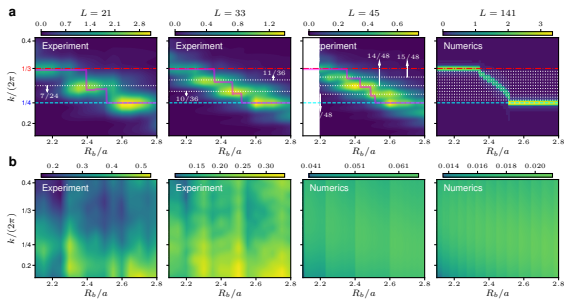


FIG. 7. **Ground-state phase diagram using von Neumann entanglement entropy.** The results for  $1 \leq R_b/a \leq 2.5$ ,  $2.5 < R_b/a \leq 3.15$ , and  $3.15 < R_b/a \leq 3.5$  are computed for systems with  $L = 288, 285$ , and  $290$ , respectively (Fig. 1b in the main text also employs this technique). Slight variations in  $L$  in different regimes ensure compatibility with the periods of the crystalline orders. The dark lobes represent crystalline orders, bounded by the bright yellow lines, show the floating phase. The bright yellow lines are BKT transition lines, separating the floating phases and the disordered phase. The boundaries between the floating phases and the crystalline orders are PT transition lines. The red line labels the direct phase transition between the  $Z_4$  order and the disordered phase, which is a chiral transition line with continuously varying critical exponents plus a single CFT point (white circle). The chiral transition line terminates at two Lifshitz points (yellow cross) where the floating phases emerge. There also exist direct phase transitions between the  $Z_0$  order and the disordered phase, which also include a single CFT point. On the equal- $k_c$  lines (cyan lines) in the disordered phase, the peak position of the structure factor  $S(k)$  remains constant at  $k_p$ . Commensurate lines, where  $2\pi/k_p$  is an integer, intersect with the  $Z_{4(6)}$  boundary at the CFT point. The floating phase fully encompasses the  $Z_3$  order, and the  $k_c = 2\pi/3$  line goes from the disordered phase into a critical phase and then into the  $Z_3$  order (see Fig. 21). White circles on the  $Z_2$  boundary denote four Ising critical points studied in Fig. 18. Triangles, squares, and the diamond represent the points discussed in the subsequent figures.



# Experimental and Numerical Fourier transforms

The floating phase is characterized by a continuous dependence in the lattice spacing (at infinite volume!).



**Figure: The structure factor for different system sizes. a**, The structure factor as a function of  $R_b/a$  is measured along the cut  $\Delta/\Omega = 3.5$  for  $L = 21, 33, 45$ . The magenta curves are peak positions from numerical results. The results for  $L = 141$  is from numerics. **b**, The structure factor is measured along the cut  $\Delta/\Omega = 0$  in the disordered phase.





# Entanglement entropy

Starting with

$$\rho_{AB} = |\text{vac.}\rangle\langle\text{vac.}|$$

We assume that the  $N_q$  qubits are split into  $N_{qA}$  and  $N_{qB}$  qubits for a bi-partition A-B. Writing the  $2^{N_q}$  dimensional vector  $c_{\{n\}}$  corresponding to the vacuum as a  $2^{N_{qA}} \times 2^{N_{qB}}$  matrix


$$C_{\{n\}_A, \{n\}_B} = c_{\{n\}},$$

we find that the reduced density matrix  $\rho_A = \text{Tr}_B \rho_{AB}$  can be written as

$$\rho_{A\{n\}_A, \{n'\}_A} = (CC^\dagger)_{\{n\}_A, \{n'\}_A},$$

in the computational basis. The von Neuman entropy is

$$S_A^{vN} = -\text{Tr}_A \rho_A \ln(\rho_A) = -\sum_m \lambda_m \ln(\lambda_m),$$

with  $\lambda_m$  the eigenvalues of  $\rho_A$  which are independent of the basis used in A. 

# Measuring entanglement entropy in a quantum many-body system

Rajibul Islam<sup>1</sup>, Ruichao Ma<sup>1</sup>, Philipp M. Preiss<sup>1</sup>, M. Eric Tai<sup>1</sup>, Alexander Lukin<sup>1</sup>, Matthew Rispoli<sup>2</sup> & Markus Greiner<sup>1</sup>

Entanglement is one of the most intriguing features of quantum mechanics. It describes non-local correlations between quantum objects, and is at the heart of quantum information sciences. Entanglement is now being studied in diverse fields ranging from condensed matter to quantum gravity. However, measuring entanglement remains a challenge. This is especially so in systems of interacting delocalized particles, for which a direct experimental measurement of spatial entanglement has been elusive. Here, we measure entanglement in such a system of itinerant particles using quantum interference of many-body twins. Making use of our single-site-resolved control of ultracold bosonic atoms in optical lattices, we prepare two identical copies of a many-body state and interfere them. This enables us to directly measure quantum purity, Rényi entanglement entropy, and mutual information. These experiments pave the way for using entanglement to characterize quantum phases and dynamics of strongly correlated many-body systems.

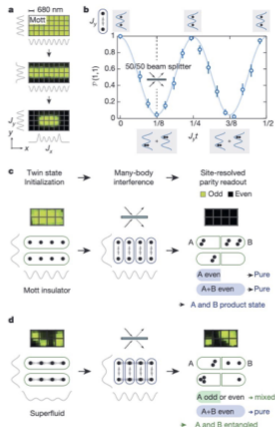


**Figure 3 | Many-body interference to probe entanglement in optical lattices.** **a**, A high-resolution microscope is used to directly image the number parity of ultracold bosonic atoms on each lattice site (in the raw images, green represents odd and black represents even). Two adjacent one-dimensional lattices are created by combining an optical lattice and potentials created by a spatial light modulator. We initialize two

# Experimental entanglement without twin copy (YM, arxiv 2404.09935)

- Preparing and interfering twin copies is not easy experimentally!
- We propose to use the entropy associated with the experimental measurements of the vacuum of a single system of entangled qubits  $S_{AB}^X$  and the reduced entropy  $S_A^X$  obtained by tracing the experimental probabilities over one half of the system.
- Using Rydberg arrays, we found from exact diagonalization and local QuEra simulations that the von Newman entanglement entropy  $S_{vN} \simeq 1.25(2S_A^X - S_{AB}^X)$ .
- The errors subtract to some extent making  $2S_A^X - S_{AB}^X$  a robust quantity.
- We conjectured that  $S_{vN} \geq 2S_A^X - S_{AB}^X$  should hold in general.



# Experimental entropy $S_{AB}^X$

Given an arbitrary prepared state  $|\psi\rangle$ , we can expand it in the computational basis

$$|\psi\rangle = \sum_{\{n\}} c_{\{n\}} |\{n\}\rangle.$$

This implies that the state  $|\{n\}\rangle$  will be observed with a probability

$$p_{\{n\}} = |c_{\{n\}}|^2.$$

These probabilities define an “experimental” (Shannon) entropy

$$S_{AB}^X \equiv - \sum_{\{n\}} p_{\{n\}} \ln(p_{\{n\}})$$

It is clear that this quantity depends on the computational basis and that it contains no information about entanglement.



# Experimental reduced entropy $S_A^X$

We can define a reduced probability in the subsystem  $A$  by tracing over  $B$ :

$$p_{\{n\}_A} = \sum_{\{n\}_B} p_{\{n\}_A\{n\}_B},$$

and define the corresponding reduced experimental entropy

$$S_A^X \equiv - \sum_{\{n\}_A} p_{\{n\}_A} \ln(p_{\{n\}_A}).$$

Again, this quantity depend on the computational basis used and cannot be identified with the von Neuman entropy  $S_A^{vN}$ . However, it is possible to show that  $S_A^X \geq S_A^{vN}$ .

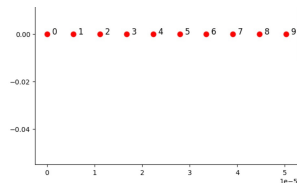
Similarly, we can define  $S_B^X$  by interchanging  $A$  ad  $B$ .



# First model calculation

$N_S=10$  chain;  $\Omega = 5\pi$  MHz;  $\Delta = 17.5\pi$  MHz;  $R_b = 8.375\mu$ ;  $A$  and  $B$  are the left and right halves so  $S_A^X = S_B^X$ .

Geometry: 10 atom chain

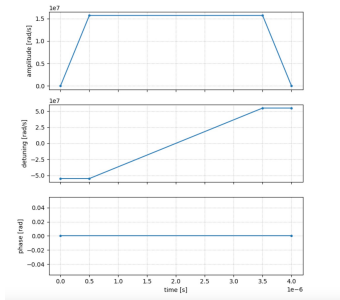


1.4

Bitstrings for 1000 shots

```
{'grgrgrgrgr': 16,  
'rggrgrgrgr': 2,  
'rgrgrgrgrr': 209,  
'rgrgrgrgr': 278,  
'rgrgrgrgr': 288,  
'rgrgrgrgr': 188,  
'rgrgrgrgrg': 19}
```

Adiabatic vacuum preparation



Average Rydberg occupations



# $S_A^{vN} \propto 2S_A^X - S_{AB}^X$ with Exact Diagonalization

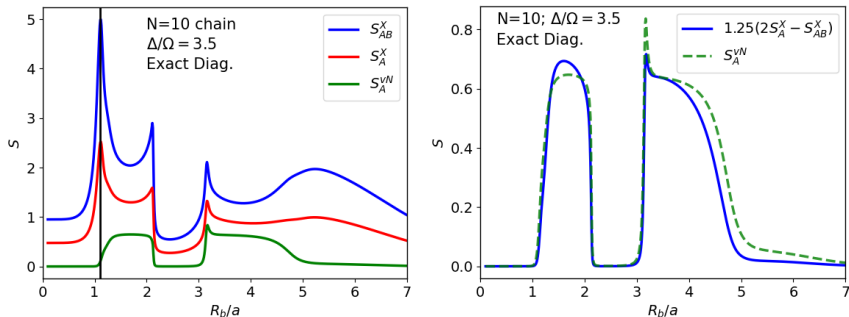


**Figure:** Entropies for a chain of 10 atoms with  $\Delta/\Omega = 3.5$  as a function of  $R_b/a_x$ . Top:  $S_{AB}^X$ ,  $S_A^X$  and  $S_A^{vN}$ ; the vertical line is at  $R_b/a_x = 1.11$ ; Bottom:  $1.25(2S_A^X - S_{AB}^X)$  and  $S_A^{vN}$ .



# Observations/Conjectures

- For large Shannon entropies:  $2S_A^X \simeq S_{AB}^X$
- In the limiting case where all the probabilities are equal to  $2^{-N_q}$ , the reduced probabilities are all equal to  $2^{-N_q/2}$  and  $2S_A^X - S_{AB}^X \rightarrow 0$ .
- This limiting case can be realized for a state which is the sum of all the computational states with equal coefficients  $2^{-N_q/2}$ . This state is a product state

$$|PS\rangle = \bigotimes_{j=0}^{N_q-1} (|0\rangle_j + |1\rangle_j) / \sqrt{2},$$

and the corresponding density matrix has zero entanglement.

- **We observed that in good approximation**

$$S_A^{vN} \propto 2S_A^X - S_{AB}^X.$$

- The important point is that it can be extracted from the bitstring measurements of a single copy of  $AB$ .





# Experiments with Aquila

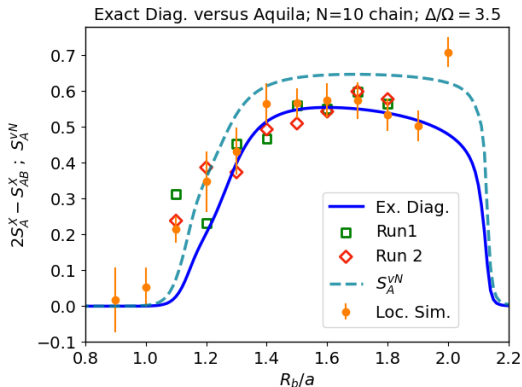


**Figure:**  $2S_A^X - S_{AB}^X$  vs.  $R_b/a_x$  with three methods: 1) exact diagonalization (continuous curve); 2) local simulator with no ramping down of  $\Omega$  at the end (filled circles), the errors bars are calculated using 10 independent runs of 1000 shots; 3) 2 runs with 1000 shots with Aquila (empty symbols);  $S_A^{vN}$  (dashed line) is also given for reference.



# Rigorous inequalities

The classical mutual information is defined as

$$I_{AB}^X \equiv S_A^X + S_B^X - S_{AB}^X.$$

It was found by Shannon that this quantity is always positive or zero.

Upper bounds can also be found by reducing  $\rho_A$  to the diagonal part  $\rho_A^X$

$$S_B^{vN} = S_A^{vN} \leq S_A^X (\text{or } S_B^X).$$

Holevo bound:

$$0 \leq I_{AB}^X \leq S_B^{vN} = S_A^{vN} \leq S_A^X (\text{or } S_B^X).$$



# Probability filtering and mutual information

YM arXiv 2404.09935 (supplementary material)

u

Method \ State	Exact	LSNRD1	LSNRD2	LSST1	LSST2	Aquila1	Aquila2
grgrgrgrgr	12	14	19	24	18	16	18
rggggrgrgr	16	21	18	< 10 (0)	< 10 (1)	15	14
rggrgrgrgr	138	142	152	201	222	136	149
rgrgggrgrgr	23	18	28	< 10 (0)	< 10 (0)	19	24
rgrgrgrggg	< 10 (6)	11	< 10 (7)	< 10 (0)	< 10 (0)	14	< 10 (5)
rgrgrgrgrgr	276	232	239	274	264	174	175
rgrgrggggr	16	14	18	< 10 (0)	< 10 (0)	19	12
rgrgrgrgrgr	276	248	244	278	266	190	180
rgrgrgrggr	138	179	168	207	200	151	179
rgrgrgrgrg	12	13	18	12	25	23	16
Total	907	892	904	996	995	804(*)	812(**)

TABLE I. States with at least 10 observations for 1000 shots. For Aquila, (\*) five additional states are not in the table: grgrgrgrgr (12), rgggrgrgrgr (12), rgggrgggrgr (12), rgrgggrggr (14), rgrgrgrgrr (11) for run 1, and (\*\*) and three additional states are not in the table: rgggrgrgrgr (12), rgggrgggrgr (11), rgrgrgrggg (12) for run 2.

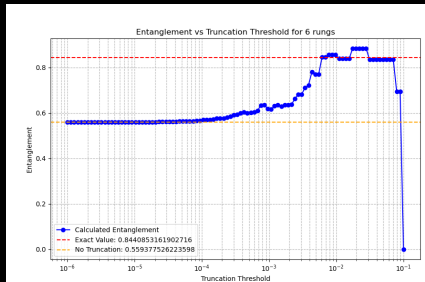
Method \ Entropy	Exact	LSNRD1	LSNRD2	LSST1	LSST2	Aquila1	Aquila2
$S_{AB}^X$	2.126	2.241	2.198	1.527	1.558	2.944	2.874
$S_{AB}^X(\text{Trunc.})$	1.6476	1.734	1.740	1.504	1.527	2.035	1.901
$S_A^X$	1.337	1.374	1.354	1.117	1.134	1.685	1.681
$S_A^X(\text{Trunc.})$	1.131	1.149	1.167	1.115	1.108	1.288	1.233
$1.25(2S_A^X - S_{AB}^X)$	0.686	0.634	0.639	0.883	0.888	0.531	0.611
$1.25(2S_A^X - S_{AB}^X)(\text{Trunc.})$	0.769	0.706	0.742	0.907	0.861	0.676	0.707

TABLE II. Entropies calculated with the full data set and truncated data sets (Trunc.) where observations with less than 10 events are discarded.



# Probabilistic filtering and mutual information

**IOWA**



Avi Kaufman

September 23, 2024



# Entanglement entropy and mutual information (ladder)

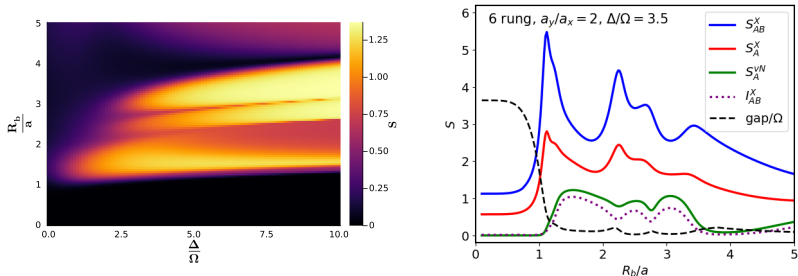


**Figure:** Left: von Neumann entanglement entropy for a six-rung ladder with  $a_y = 2a_x$  as a function of  $R_b/a_x$  and  $\Delta/\Omega$ . Right: Comparison of  $S_{AB}^X$ ,  $S_A^X$ ,  $S_A^{vN}$  and  $I_{AB}^X$  at a fixed  $\Delta/\Omega = 3.5$ .



# Effect of low probability truncation (filtering)

arXiv 2411.07092 with A. Kaufman, J. Corona, Z. Ozzello, and M. Asaduzzaman (Asad). Truncation: remove states with  $p \leq p_{min}$  and renormalize.

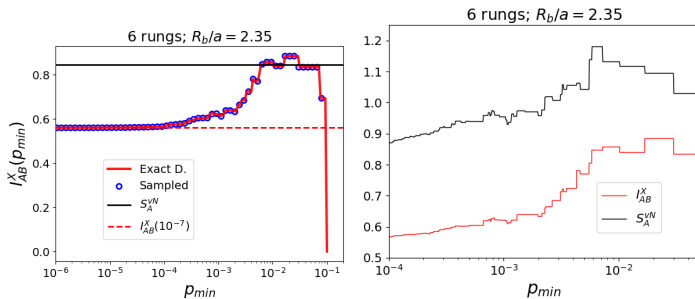


**Figure:** Left:  $I_{AB}^X(p_{min})$  for a six-rung ladder with exact diagonalization (continuous line) and DMRG sampling (open circles). Right:  $I_{AB}^X(p_{min})$  and  $S_A^{vN}(p_{min})$  for a six-rung ladder with exact diagonalization. The ground state is also modified if we remove the corresponding states and renormalize so  $I_{AB}^X(p_{min}) \leq S_A^{vN}(p_{min})$  and no contradiction.



# Effect of size and lattice spacing

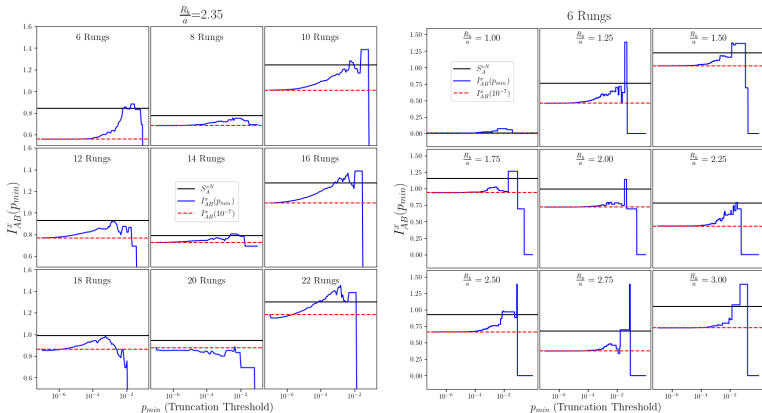


**Figure:** Effects of the system size on  $I_{AB}^X(p_{min})$  for 6, 8, ..., 22 rungs,  $R_b/a = 2.35$  and 10 million counts obtained via DMRG. Effects of the lattice spacing on  $I_{AB}^X(p_{min})$  for  $R_b/a = 1.0, 1.25, \dots, 3.0$ , 6 rungs and 10 million counts obtained via DMRG.



# Filtered Aquila data (M. Asaduzzaman)

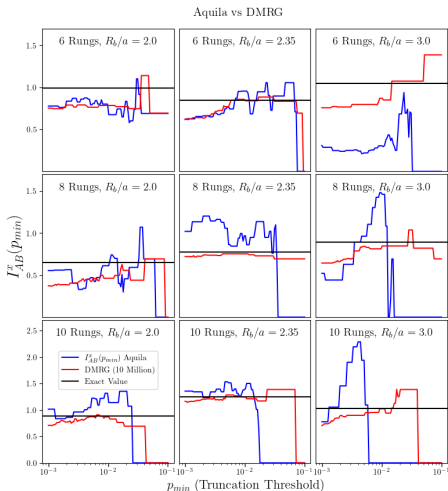


**Figure:** Filtered mutual information obtained from DMRG (10 million counts) vs Aquila (1000 shots) for varying  $Rb/a$  and system sizes.





# Distribution of probability values

- When the computational basis has a large dimension, many states have a low probability.
- We define the number of states  $NS(p, dp)$  having a probability between  $p - dp/2$  and  $p + dp/2$ .
- For systems large enough and bins small but not too small, it is tempting to try to use a continuous approximation

$$NS(p, dp) \simeq \mathcal{N}_{lin.}(p)dp.$$

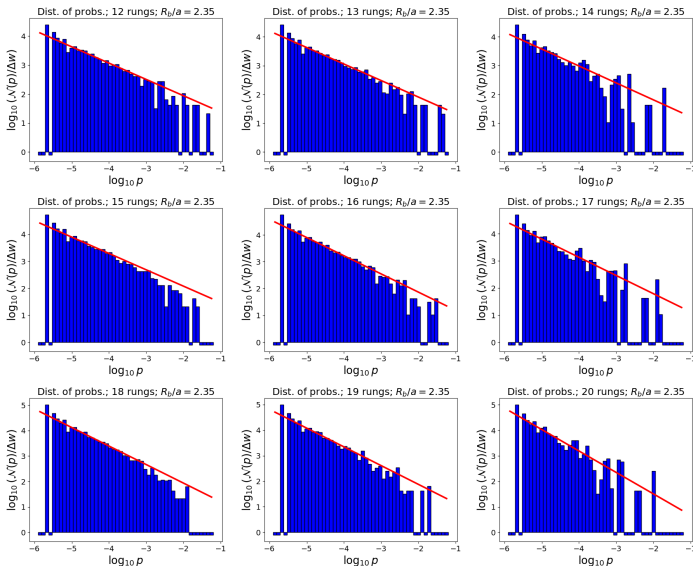
- In the following, we will see that in good approximation for small  $p$ ,

$$\mathcal{N}_{lin.}(p) \simeq Cp^{-1-\zeta},$$

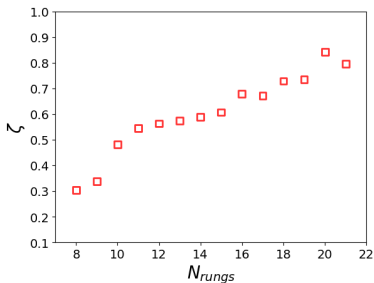
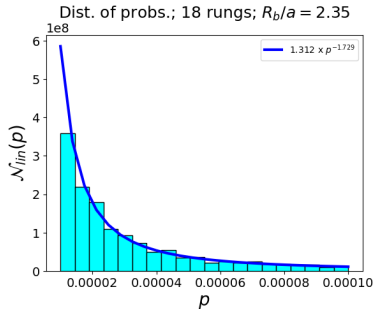
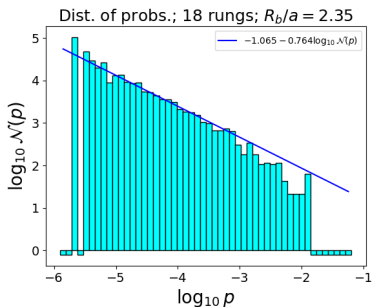
- If we assume that in the infinite volume limit, the power behavior extends to arbitrarily small values of  $p$ , then the normalization of the probability requires that  $\zeta < 1$ .
- What should we do if  $\zeta \geq 1$ ?



# log-log fits (using J. Corona DMRG sampling)



# $\mathcal{N}_{lin.}(p) \simeq Cp^{-1-\zeta}$ (preliminary)



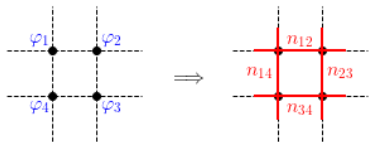
# TLFT: From compact to discrete (O(2) example)

$$Z_{O(2)} = \prod_X \int_{-\pi}^{\pi} \frac{d\varphi_X}{2\pi} e^{\beta \sum_{x,\mu} \cos(\varphi_{x+\hat{\mu}} - \varphi_x)} = \text{Tr} \prod_X T_{n_{x-\hat{1},1}, n_{x,1}, \dots, n_{x,D}}^{(X)}$$

$$e^{\beta \cos(\varphi_{x+\hat{\mu}} - \varphi_x)} = \sum_{n_{x,\mu}=-\infty}^{\infty} e^{in_{x,\mu}\varphi_{x+\hat{\mu}}} l_{n_{x,\mu}}(\beta) e^{-in_{x,\mu}\varphi_x}$$

$$\text{Tensor : } T_{n_{x-\hat{1},1}, n_{x,1}, \dots, n_{x-\hat{D},D}, n_{x,D}}^{(X)} = \sqrt{l_{n_{x-\hat{1},1}} l_{n_{x,1}} \dots l_{n_{x-\hat{D},D}} l_{n_{x,D}}} \times \delta_{n_{x,\text{out}}, n_{x,\text{in}}}$$

$$\prod_X \int_{-\pi}^{\pi} d\varphi_X \implies \sum_{\{n\}}$$



The gauged version is the Abelian Higgs model.



# Introductions to Tensor Lattice Field Theory

REVIEWS OF MODERN PHYSICS, VOLUME 94, APRIL–JUNE 2022

## Tensor lattice field theory for renormalization and quantum computing

Yannick Meurice

Department of Physics and Astronomy, The University of Iowa, Iowa City, Iowa 52242, USA

Ryo Sakai

Department of Physics and Astronomy, The University of Iowa, Iowa City, Iowa 52242, USA  
and Department of Physics, Syracuse University, Syracuse, New York 13244, USA

Judah Unmuth-Yockey

Department of Physics, Syracuse University, Syracuse, New York 13244, USA  
and Fermi National Accelerator Laboratory, Batavia, Illinois 60510, USA

(published 26 May 2022)

The successes and limitations of statistical sampling for a sequence of models studied in the context of lattice QCD are discussed and the need for new methods to deal with finite-density and real-time evolution is explained. It is shown that these lattice models can be reformulated using tensorial methods where the field integrations in the path-integral formalism are replaced by discrete sums. These formulations involve various types of duality and provide exact coarse-graining formulas that can be combined with truncations to obtain practical implementations of the Wilson renormalization group program. Tensor reformulations are naturally discrete and provide manageable transfer matrices. Truncations with the time continuum limit are combined, and Hamiltonians suitable for performing quantum simulation experiments, for instance, using cold atoms, or to be programmed on existing quantum computers, are derived. Recent progress concerning the tensor field theory treatment of noncompact scalar models, supersymmetric models, economical four-dimensional algorithms, noise-robust enforcement of Gauss's law, symmetry preserving truncations, and topological considerations are reviewed. Connections with other tensor network approaches are also discussed.

DOI: 10.1103/RevModPhys.94.025005

### CONTENTS

I. Introduction	2	D. Exact blocking	19
II. Lattice Field Theory	4	VI. Tensor Renormalization Group	20
A. The Kogut sequence: From Ising to QCD	4	A. Block spinning through SVD	20
B. Classical lattice models and path integral	4	B. Optimized truncations	20
C. Physical applications	7	C. Higher-dimensional algorithms	22
D. Computational methods beyond perturbation theory	7	D. Observables with tensors	22
III. Quantum Computing	8	E. Niemeijer-van Leeuwen equation	23
A. Situations where importance sampling fails	8	F. A simple example of TRG fixed point	24
B. Qubits and other quantum platforms	8	G. Corner double line structure on tensor network	25
C. From Euclidean transfer matrices to Hilbert spaces	9	VII. Tensors for Spin Models with	25
D. Topological and geometrical dualities	10	A. Abelian Symmetry	25
E. Real-time evolution with qubits	12	A. $O(2)$ nonlinear sigma model	25
F. Lloyd-Suzuki/Trotter product formula	12	B. $q$ -state clock models	26
G. Dealing with noise in the NISQ era	13	C. Dual reformulations with unconstrained variables	27
H. Quantum computations and simulations	14	D. Chemical potential, complex temperature, and importance sampling	27
1. Ising model	14	VIII. Tensors for Spin Models with Non-Abelian	27
2. Gauge theories	14	Symmetries	27
IV. The Meaning of Quantum versus Classical	15	A. $O(3)$ nonlinear sigma model	27
A. Models	15	B. $SU(2)$ principal chiral model	29
B. Phase transitions	15	C. Truncations and asymptotic freedom	30
C. Tensor networks	15	IX. Tensors for Lattice Gauge Theories	31
V. Tensor Methods Explained with the Ising Model	16	A. Pure gauge $U(1)$	31
A. Tensor formulation	16	1. Discrete Maxwell equations	31
B. The forms of duality	18	2. Abelian gauge duality	32
C. Boundary conditions	18	B. The compact Abelian-Higgs model	32
		C. $SU(2)$ gauge theory	33

IOP Publishing | Bookstore

Home | Quantum Field Theory

## Quantum Field Theory

A quantum computation approach

Yannick Meurice



# Interdisciplinary effort

SVD and TN methods developed in condensed matter (T. Nishino, X-G. Wen, M. Levin, Tao Xiang, ...). Character expansions used in strong coupling expansions (C. Itzykson, ...). Cutting edge effort in Japan: S. Akiyama, D. Kadoh, Y. Kuramashi, R. Sakai, S. Takeda, Y. Yoshimura, ...

INT WORKSHOP INT-21R-1C

## Tensor Networks in Many Body and Quantum Field Theory

April 3, 2023 - April 7, 2023

### ORGANIZERS

#### Simon Catterall

Syracuse University  
smcatterall@gmail.com

#### Glen Evenbly

Georgia Institute of Technology  
glen.evenbly@gmail.com

#### Yannick Meurice

University of Iowa  
annick-meurice@uiowa.edu

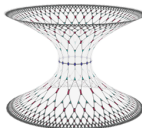
#### Alessandro Roggero

University of Washington  
roggero@uw.edu

### DIVERSITY COORDINATOR

#### Alessandra Roggero

University of Washington  
roggero@uw.edu



APPLICATION FORM - FOR  
FULL CONSIDERATION,  
APPLY BY NOVEMBER 27,  
2022

### OVERVIEW

*Note to applicants: This is an in-person workshop. There is no virtual/online option for this event at this time. Please be aware that all participants must show proof of vaccination against COVID-19 upon arrival to the INT.*

*Disclaimer: Please also be aware that due to ongoing concerns regarding the COVID-19 pandemic, the workshop may be cancelled.*

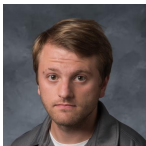
Tensor network methods are rapidly developing and evolving in many areas of



# Gaussian Wave Packets (Michael Hite)

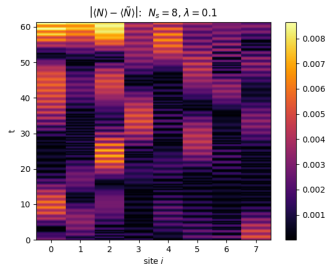
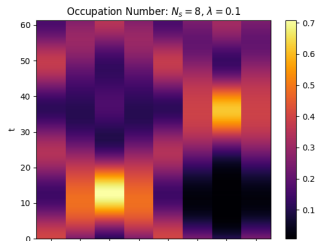
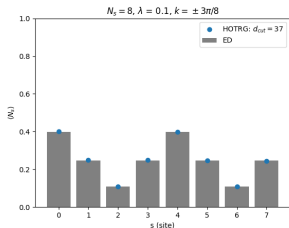
arXiv 2411.05301

## Michael Hite: Two-particle Scattering



$$\hat{H} = - \sum_{j=0}^{N_s-1} (\lambda \hat{\sigma}_j^x \hat{\sigma}_{j+1}^x + \hat{\sigma}_j^z)$$

- Initialize a right moving wave packet centered at site 0 and left moving wave packet centered at site 4.



# Principal chiral model in 2+1 D



JLAB-THY-24-4047, UTCCS-P-154, FERMLAB-PUB-24-0308-T

## $SU(2)$ principal chiral model with tensor renormalization group on a cubic lattice

Shinichiro Akiyama <sup>1,2,\*</sup>, Raghav G. Jha <sup>3,†</sup> and Judah Unmuth-Yockey <sup>4,‡</sup>

<sup>1</sup>Center for Computational Sciences, University of Tsukuba, Tsukuba, Ibaraki 305-8577, Japan

<sup>2</sup>Graduate School of Science, The University of Tokyo, Bunkyo-ku, Tokyo, 113-0033, Japan

<sup>3</sup>Thomas Jefferson National Accelerator Facility, Newport News, Virginia 23606, USA

<sup>4</sup>Fermi National Accelerator Laboratory, Batavia, Illinois, USA

We study the continuous phase transition and thermodynamic observables in the three-dimensional Euclidean  $SU(2)$  principal chiral field model with the triad tensor renormalization group (tTRG) and the anisotropic tensor renormalization group (ATRG) methods. Using these methods, we find results that are consistent with previous Monte Carlo estimates and the predicted renormalization group scaling of the magnetization close to criticality. These results bring us one step closer to studying finite-density QCD in four dimensions using tensor network methods.



1 2024

## Tensor renormalization group for fermions

Shinichiro Akiyama (Tsukuba U., CCS and Tokyo U., ICEPP), Yannick Meurice (Iowa U.), Ryo Sakai (Tokyo U.)

Jan 16, 2024

47 pages

Published in: *J.Phys.Condens.Matter* 36 (2024) 34, 343002

Published: May 28, 2024

e-Print: 2401.08542 [hep-lat]





# Conclusions

- QC/QIS in HEP and NP: big goals with many intermediate steps
- Tensor Lattice Field Theory (TLFT): generic tool to discretize path integral formulations of lattice model with compact variables (truncations preserve symmetries).
- Ladder-shaped Rydberg arrays with two (or three) atoms per site proposed as simulators for the compact Abelian Higgs model.
- Matching between simulator and target model should be understood in the continuum limit (universal behavior).
- Effective Hamiltonians for the simulator: same three types of terms as the target model plus an extra quartic term.
- The two-leg ladder has a very rich phase diagram that can be studied with the mutual information.
- Implementations with AWS/QuEra
- Progress with hybrid hadronization, evolution in AdS.
- Thanks for listening!
- For questions, email: [yannick-meurice@uiowa.edu](mailto:yannick-meurice@uiowa.edu) .



Thanks for listening!



Figure: Isingized version of Yukawa

